ELSEVIER

Fusion Engineering and Design 30 (1995) 339–356

Fusion Engineering and Design

Modeling of fully-developed, liquid metal, thin film flows for fusion divertor applications

Neil B. Morley, Mohamed A. Abdou

43-133 Engineering IV, Mechanical, Aerospace and Nuclear Engineering Department, University of California, Los Angeles, Box 951597, Los Angeles, CA 90024-1597, USA

Received February 1995; revised 8 March 1995

Handling Editor: M. Abdou

Abstract

Interest in thin film flows of liquid metal (LM) in a strong magnetic field has increased due to the possible application of such flows to the protection of divertor surfaces in a tokamak fusion reactor. In order to investigate the behavior of such a thin film flow in the fully-developed limit, a two-dimensional numerical model of open-channel, magnetohydrodynamic (MHD) flow has been constructed. This flow is contained in a chute of arbitrary electrical conductance with a magnetic field perpendicular to the flow direction but with arbitrary azimuthal orientation. Results of this self-consistent model are used to examine issues of importance to the successful fusion divertor application of thin film flow, such as the uniform film height and heat transfer of the films. It is seen that the flow height can be dominated by even a small transverse component of the field, rather than the stronger coplanar component, due to the elongated nature of the film. The model is also used to determine the validity of the Hartmann-averaging technique, an approximation used extensively in previous developing film models to account for the effects of a dominant coplanar field. This Hartmann-averaging is shown to be accurate in predicting the behavior of the core flow in the strong coplanar MHD interaction regimes, but cannot predict the flow quantity in parallel layer jets that can make up an appreciable portion of the flow. The Hartmann-averaging method is seen to be unsuitable for elongated flows dominated by the transverse field component.

1. Introduction

The use of a liquid metal (LM) film flowing down an inclined plate has been proposed [1] as a self-healing, self-cooling, tokamak divertor surface. The LM film divertor has several potential benefits for reactor performance, including:

- protection of the underlying surface from physical erosion and surface blistering;
- a continually replenished surface that replaces eroded materials;
- a large heat removal capability that may eliminate the need for a separate coolant;
- reduced heat penetration to the structure, thus reducing thermal stresses;
- elimination of armor-tile attachment complications;

SSDI 0920-3796(95)00417-0

- possible reduction in the large tritium inventories trapped in immobile armor materials; and
- possible elimination of the usage of large amounts of beryllium as a plasma facing material.

Although LM film divertors can in principle eliminate several of the major existing problems in the development of solid surface plasma facing components, the use of LM film in this capacity adds unique problems of its own. For example, concerns about contamination of the main plasma from rapidly eroded LM material have yet to be addressed to a satisfactory degree [2]. Also, the effect of the plasma wind on the free surface shape is expected to be significant [3,4], especially for lithium films, but not necessarily catastrophic.

Equally serious, however, is the behavior of the LM film in the complicated magnetic fields near a tokamak divertor. The ability to establish and maintain a stable film with the appropriate film height and velocity is crucial to the success of this design concept. An investigation of the behavior of the fully-developed film in a channel of arbitrary electrical conductance and in a spatially oblique magnetic field is the focus of this work. The model is presented briefly in Section 2, and results are used to answer the following questions in Sections 3 and 4.

- Is it possible to create a desirable uniform flow?
- Is the use of various simplifying techniques to reduce the complexity of developing film models valid?

A more detailed investigation of the two-dimensional velocity and induced magnetic field (electric current) profiles of uniform flow is the subject of a separate paper [5]. Certainly other magnetohydrodynamic (MHD) issues exist, such as the effect of temporal and spatially variable magnetic fields, but this initial investigation is essential in understanding the nature of LM MHD thin film flows.

2. Fully-developed film flow model

The flow of liquid metal in a magnetic field is governed by the standard MHD equations which include: the Navier–Stokes equation of momentum conservation, the mass continuity equation, Ohm's law, and Maxwell's equations. The so-called induction equation used in this model is obtained by taking the divergence of Ohm's law and applying Maxwell's equations. It is more commonly used in formulations that solve for the induced magnetic field instead of the current density. See Ref. [6] for a detailed treatment of the LM–MHD equations as applied to flow in closed ducts.

The typical quasi-coplanar geometry (Fig. 1) as defined in Ref. [7] has the applied field direction dominantly parallel to z, which lies in the plane of the film but perpendicular to the main flow direction, with smaller components in the other two directions. The x coordinate denotes the direction of dominant fluid flow and is termed longitudinal. The y coordinate is normal to the substrate and is named the transverse direction. Other definitions include: h as the film height measured along y, θ as the angle of the substrate to the horizon (measured positive for downward sloping chutes), α as the angle of the magnetic induction to z, and finally a as the channel width with the chute walls located at $\pm a/2$. This type of flow is indicative of a poloidally flowing divertor film where the main toroidal field component is largely aligned with z.

The MHD equations are simplified with the assumption of an open-channel, laminar, fully-developed flow of a uniform depth over the channel width. As a consequence of the fully-developed assumption, the total pressure distribution is hydrostatic and the height of the flow is no longer changing as it proceeds down the channel (uniform flow). The velocity has only the longitudinal component, $\vec{v} = (u, 0, 0)$ as a result of the driving force of gravity. These same assumptions lead to the inclusion of only the x component of the

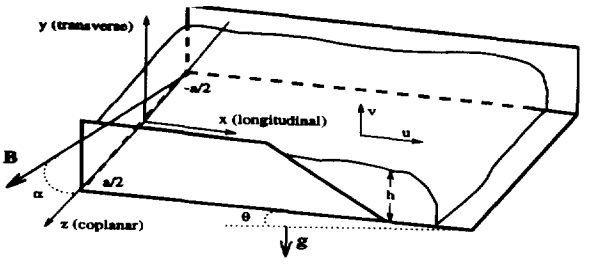

Fig. 1. Geometry of quasi-coplanar LM film flow.

induced field as well, $\vec{B}^{t} = (B^{t}_{x}, 0, 0)$, where the total field is the sum of the originally applied field and $\vec{B}^{i}$ induced by the motion of the flow. Also, in this analysis we further simplify the magnetic geometry by the neglect of the longitudinal component of the applied field so that it can be defined as $\vec{B}^{a} = (0, B^{a}_{y}, B^{a}_{z})$. The longitudinal component tends to produce forces that lead to a non-uniform surface height (in z) and small motion in the y and z directions, but should not effect the main film velocity drastically in fully-developed flow. Its inclusion would require significantly more effort to model, and so is neglected in this approximate treatment.

The application of these simplifying assumptions reduces the general equations to the following system in terms of the velocity, induced magnetic field, volumetric flowrate and the uniform film height:

$$\nabla^{2}_{\perp} u + \frac{1}{\rho \mu_{m} \nu} (\vec{B}^{a} \cdot \nabla_{\perp}) B^{t}_{x} = -\frac{g \sin \theta}{\nu} \tag{1}$$

$$\nabla^{2}_{\perp} B^{t}_{x} + \mu_{m} \sigma_{f} (\vec{B}^{a} \cdot \nabla_{\perp}) u = 0 \tag{2}$$

$$\int_{-a/2}^{a/2} \int_{0}^{h} u \, dy \, dz = Q \tag{3}$$

where the operator $\nabla_{\perp}$ is defined as $(0, \partial/\partial y, \partial/\partial z)$, g is the acceleration of gravity and Q is the volumetric flowrate. The symbols σ_f, ρ, ν and μ_m are electrical conductivity, mass density, kinematic viscosity and magnetic permeability of the LM. The constancy of these material properties is assumed throughout this work. The constant flowrate condition is given as the third equation of the fully-developed model formulation. It is required if the uniform film height h is to be computed. Eq. (3) is coupled to Eqs. (1) and (2) through the boundary conditions since h is the upper limit of the solution space for the velocity and induced field profiles. If h is assumed a priori then Eq. (3) is needed only to compute the flowrate that results in such a uniform film height.

The boundary conditions for the velocity are no-slip on the channel walls, and free-slip at the free surface:

$$u = 0 \qquad \text{at } y = 0 \text{ or } z = \pm a/2 \tag{4}$$

$$\frac{\partial u}{\partial y} = 0 \qquad \text{at } y = h \tag{5}$$

The conditions needed for the induced field can be determined from the thin conducting wall boundary conditions [6,8]:

$$\left(\frac{\sigma_s a_s}{\sigma_f}\right) \frac{\partial B^{i}_{x}}{\partial z} \pm B^{i}_{x} = 0 \qquad \text{at } z = \pm a/2 \tag{6}$$

$$\left(\frac{\sigma_b a_b}{\sigma_f}\right) \frac{\partial B^{i}_{x}}{\partial y} - B^{i}_{x} = 0 \qquad \text{at } y = 0 \tag{7}$$

$$B^{i}_{x} = 0 \qquad \text{at } y = h \tag{8}$$

where the subscripts b and s refer to the bottom wall and the widewalls respectively. The thin conducting wall approximation treats the channel walls like an infinitely thin conductor with no voltage difference over the width of the wall. It is accurate provided that the resistance of the wall width is small compared to the resistance of the entire current path through the walls.

Eqs. (1)–(3) and the boundary conditions are normalized using the following characteristic quantities and dimensionless parameters.

$$y_* = h, \qquad z_* = a/2 \tag{9}$$

$$u_* = \left(\frac{a}{2}\right)^{2} \frac{g \sin \theta}{\nu}, \qquad B^{t}_{*} = u_* \mu_m (\sigma_f \nu \rho)^{1/2}, \qquad Q_* = 2(a/2)^{2} u_* \tag{10}$$

$$\mathrm{Ha} = B^{a}(a/2)\left(\frac{\sigma_f}{\rho \nu}\right)^{1/2}, \qquad \Phi_{s,b} = \frac{a_{ws,b} \cdot \sigma_{ws,b}}{(a/2)\sigma_f}, \qquad \beta = \frac{h}{a/2} \tag{11}$$

The choice of the characteristic velocity and induced field may seem rather cryptic, but are in reality very telling. The characteristic induced field is simply that expected for a completely insulated channel instead of that of a perfectly conducting channel which is normally used. The characteristic velocity when multiplied by β^2 is the velocity at which friction from the backing plate balances the driving force of gravity. So if $u/u_* < \beta^2$ for a thin film flow, the MHD forces are beginning to affect the flow. If $u/u_* \ll \beta^2$, the MHD forces are dominating friction forces.

Denoting the dimensionless variables with a tilde, the new set of equations is:

$$\frac{\partial^2\tilde{u}}{\partial\tilde{y}^2}+\beta^2\frac{\partial^2\tilde{u}}{\partial\tilde{z}^2}+\mathrm{Ha}\beta\left(\sin\alpha\frac{\partial\tilde{b}}{\partial\tilde{y}}+\beta\cos\alpha\frac{\partial\tilde{b}}{\partial\tilde{z}}\right)=-\beta^2 \tag{12}$$

$$\frac{\partial^2\tilde{b}}{\partial\tilde{y}^2}+\beta^2\frac{\partial^2\tilde{b}}{\partial\tilde{z}^2}+\mathrm{Ha}\beta\left(\sin\alpha\frac{\partial\tilde{u}}{\partial\tilde{y}}+\beta\cos\alpha\frac{\partial\tilde{u}}{\partial\tilde{z}}\right)=0 \tag{13}$$

$$\frac{\beta}{2}\int_{-1}^{1}\int_{0}^{1}\tilde{u}\,\mathrm{d}\tilde{y}\,\mathrm{d}\tilde{z}=\beta\tilde{u}_{\mathrm{ave}}=\tilde{Q} \tag{14}$$

The choice of this normalization leaves the differential operators on the left hand side of Eqs. (12) and (13) identical. Adding and subtracting the two equations reforms this system into

$$\frac{\partial^2\omega_{\pm}}{\partial\tilde{y}^2}+\beta^2\frac{\partial^2\omega_{\pm}}{\partial\tilde{z}^2}\pm\mathrm{Ha}\beta\times\left(\sin\alpha\frac{\partial\omega_{\pm}}{\partial\tilde{y}}+\beta\cos\alpha\frac{\partial\omega_{\pm}}{\partial\tilde{z}}\right)=-\beta^2 \tag{15}$$

where $\omega_{\pm}=\tilde{u}\pm\tilde{b}$. Although the equations for ω_+ and ω_- are decoupled, the new variables are related now through coupled boundary conditions. These new boundary conditions are:

$$\omega_-+\omega_+=0 \qquad \text{at } \tilde{y}=0 \text{ or } \tilde{z}=\pm1 \tag{16}$$

$$\frac{\partial\omega_-}{\partial\tilde{y}}+\frac{\partial\omega_+}{\partial\tilde{y}}=0 \qquad \text{at } \tilde{y}=1 \tag{17}$$

$$\omega_+-\omega_-=0 \qquad \text{at } \tilde{y}=1 \tag{18}$$

$$\Phi_s\left(\frac{\partial\omega_+}{\partial\tilde{z}}-\frac{\partial\omega_-}{\partial\tilde{z}}\right)\pm(\omega_--\omega_+)=0 \qquad \text{at } \tilde{z}=\pm1 \tag{19}$$

$$\frac{\Phi_b}{\beta}\left(\frac{\partial\omega_+}{\partial\tilde{y}}-\frac{\partial\omega_-}{\partial\tilde{y}}\right)-(\omega_--\omega_+)=0 \qquad \text{at } \tilde{y}=0 \tag{20}$$

With these boundary conditions the non-dimensional system is complete. The governing parameter set is effectively reduced to Ha, $\Phi_{s,b}$, α, and either $\tilde{Q}$ or β. If β is given as an input, then Eq. (14) is required only to compute the necessary flowrate, and the system is reduced to only Eqs. (12)–(13). From this point on, the tildes will be dropped from the equations for convenience. When the discussion reverts to any dimensional considerations, this fact will be noted in the text and the tildes reinstated for clarity.

Eq. (15) is solved numerically as pseudo-heat conduction/convection equations with coupled boundary conditions. The derivatives are finite differenced with a split operator scheme, where second order derivatives are second order central differenced while first order derivatives use a combination of central and upwind differencing. The upwind method used here is only first order accurate with respect to the grid size, but provides more physically realistic solutions than second order central differences when the cell Peclet number is greater than two [9]. The occurrence of false diffusion [9, p. 106] when the grid is not aligned with the pseudo-convection velocity is expected for this scheme. This will result in some smearing out of sharp gradients in $\omega_\pm$ when $\alpha\neq0$. This false diffusion is reduced by the use of the finest possible grid spacing in the interior region for cases with oblique applied magnetic field.

The simple grid constructed for this problem is an unequally spaced rectangular mesh. A small grid spacing is selected for near the walls, and a larger spacing is used for the interior. The grid generation routine written for this problem allows the user to choose the boundary layer size on each wall, the maximum cell size and the maximum ratio of size from one cell to the next. The actual choice of grid spacing and total number of grid points is dependent on the particular problem due to the variable width of boundary layers and the conductivity of the walls. In general, runs with insulated walls and low Hartmann numbers (Ha $\approx$ 1000) may utilize around 60 × 60 grids, where conducting walls with larger Ha could require grids with 200 or more grid points in each direction to adequately resolve the boundary layers and interior shear layers. The dependency of the solutions on the grid selection is minimal once adequate resolution of the boundary layers is achieved. For oblique fields, this condition requires many interior grid points to resolve shear layers not exactly aligned with the grid.

Two variations of the solution method were coded, FDFF solves the problem with the value of β given, and then, at the end, computing the required Q from Eq. (14). FDBV solves for β as

Table 1
Values of parameters typical of reactor environment flows

Symbol	ITER (Ga as working LM)	
	Min	Max
a 2 (cm)	10	50
h_o (mm)	2	6
B^a (T)	5	10
u_o (m s^{-1})	1	5
θ (°)	5	70
α (°)	0	15
Ha	2×10^4	2×10^5
Re_o	6×10^3	1×10^5
Fr_o	50	425
β_o	0.004	0.06
$\bar{Q}$	5×10^{-10}	1×10^{-5}

well, after each pass recomputing β from Eq. (14) using the given Q. FDFF converges faster as a result of the reduced number of variables in the solution set. The two codes give consistent answers to equivalent problems and accurately converge to known analytic solutions in the limit of large or small β [5] and in the limit of strong MHD interaction [10]. Further details of the numerical methods can be found in [5,8]. Results from either code will be called FDFF and are not necessarily produced by the FDFF code variant.

3. Fusion relevant results of FDFF model

The goal of this section is not to thoroughly explore all the implications of the FDFF model, but rather to introduce some fusion considerations in varying degrees of detail. For example, the heat transfer, which is as rich as topic as the determination of the flow fields in general, is not analyzed in great depth. Instead, more qualitative remarks are given to serve as guidelines for future, fusion-related research topics. Readers are referred to Ref. [5] for more in-depth discussion of the flow fields presented.

ITER relevant parameter ranges are summarized in Table 1. The channel sizes are rather wide in order to cover the large divertor area in as few segments as possible. The inlet velocities and film inlet heights are estimated from the literature as those required to adequately protect the surface and remove the deposited energy [11–13]. The field strength depends on the location of the divertor, where inboard divertors will see a larger field than their outboard counterparts. The maximum angle of inclination is limited to avoid the wavy surface flow predicted to worsen for steep to vertical film flows. The field is expected to suppress these waves to some degree, but probably not entirely. The maximum inclination of 70° is selected rather arbitrarily as an approximate balance of these two tendencies, but the precise limit must be investigated further. The o subscript denotes values at the inlet, which may change as the film proceeds down the channel.

Before continuing with this discussion, a classification of flow regimes based on FDFF results is in order. Depending on the orientation of the field in flows with small β, the flow can be dominated by either the y or z component of the applied field.

- Regime 1: dominated by viscosity
  $\mathrm{Ha}\beta \sin\alpha,\ \frac{1}{2}\mathrm{Ha}\beta^2 \cos\alpha < 1$
- Regime 2: dominated by y field
  $\mathrm{Ha}\beta \sin\alpha > 10,\ \frac{1}{2}\mathrm{Ha}\beta^2 \cos\alpha$
- Regime 3: dominated by z field
  $\frac{1}{2}\mathrm{Ha}\beta^2 \cos\alpha > 50,\ \mathrm{Ha}\beta \sin\alpha$

These regimes are shown graphically in Fig. 2. The flow channel itself is subdivided into three regions labeled I, II and III, and shown in Fig. 3 for each flow regime. The transition between regime 2 and regime 3 occurs when a single field line intersects both the lower-left and the upper-right corner of the channel, occurring when $\beta = 2 \tan\alpha$. At this point, region I dominated by the y field in regime 2 disappears entirely, reappearing in regime 3 flow dominated by z field component.

3.1. Laminar flow

The FDFF model relies on the assumption of laminar flow. A quick check of this condition using the values in Table 1 is therefore in order. For duct flow, the laminarization limit for flow elongated along the field is given in Ref. [6] as

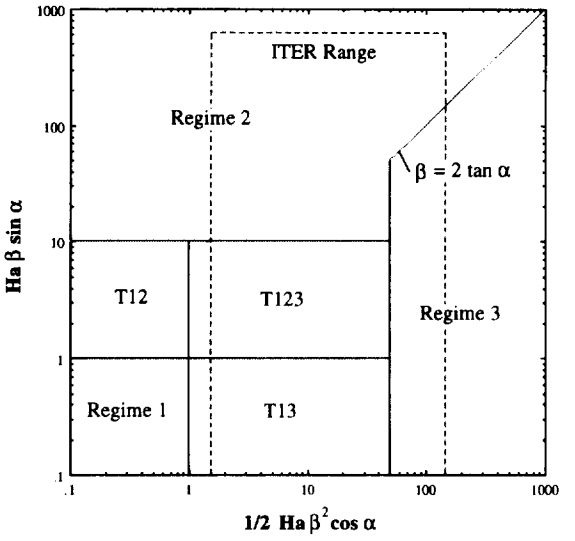

Fig. 2. Flow regime parameter space. T12 is the transition between regimes 1 and 2 flow. T13 is the transition between regimes 1 and 3 flow. T123 has elements of all regimes, and the ITER range is determined from Table 1.

$$\mathrm{Ha}\beta/\mathrm{Re} = \frac{B^{a}}{u_{ave}}\left(\frac{\sigma_f \nu}{\rho}\right)^{1/2} > 7.7 \times 10^{-3} \qquad (21)$$

Using worst case values from Table 1 we compute $\mathrm{Ha}\beta/\mathrm{Re} = 1.35 \times 10^{-2}$ for ITER using gallium as the working metal. This is about twice the limit value, indicating laminar flows over the range of parameters considered.

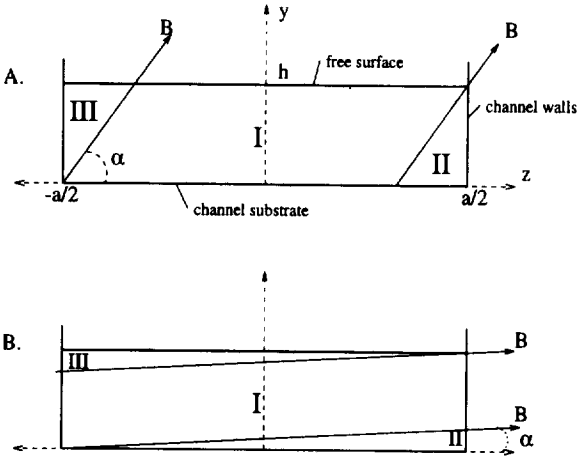

Fig. 3. Channel regions for (a) regime 2 and (b) regime 3 flow.

3.2. Heat transfer

The velocity profile of the flowing film is important to know for a variety of reasons. Primarily the velocity profile will be used in heat transfer calculations to determine temperature profiles and total heat removal capability of a specific divertor design. Most heat transfer calculations made for film heat removal and temperature profiles have used slug flow for the velocity profile [11,12]. For fast films (films flowing fast enough to remove all incident energy), it has previously been shown in the above references that heat conduction limits the depth to which the heat flux penetrates into the film during the time it is exposed to the plasma. Increasing the flow height provides greater protection against off-normal conditions like disruptions, but does not increase the overall heat removal capability in the strike zone before the surface temperature limit is reached. Of course, if conduction in the transverse direction could be enhanced by the presence of turbulence, flow or boundary layer instabilities or mixing due to the momentum of the plasma striking the surface, then this claim may not be strictly true.

Despite the lack of sensitivity of the heat removal to the film height, the velocity profile does affect the heat removal. The possibility exists for flows with large velocity jets on the free surface. These jets will improve the overall heat transfer capability of the thin films. For the same average velocity, the heat flux will see a faster moving layer on the heated surface (in the center of the channel), increasing the heat removal capability of the film in this region. Near the sidewalls, however, the velocity can drop to zero parabolically, reducing the heat removal in these areas as compared with that calculated with slug flow. A comparison of surface velocities for several different cases normalized with their average velocities is shown in Fig. 4.

If oblique fields are considered, the surface velocities profiles can vary dramatically depending on the wall conductance. For insulated channels, the reshaping of the surface jet to a more triangular shape will shift the area of better heat transfer to one side of the channel instead of directly in the middle. If the flow is in regime 2, where the y component of the field dominates, the flow is pretty close to the slug flow profile, except in region III where the velocity drops.

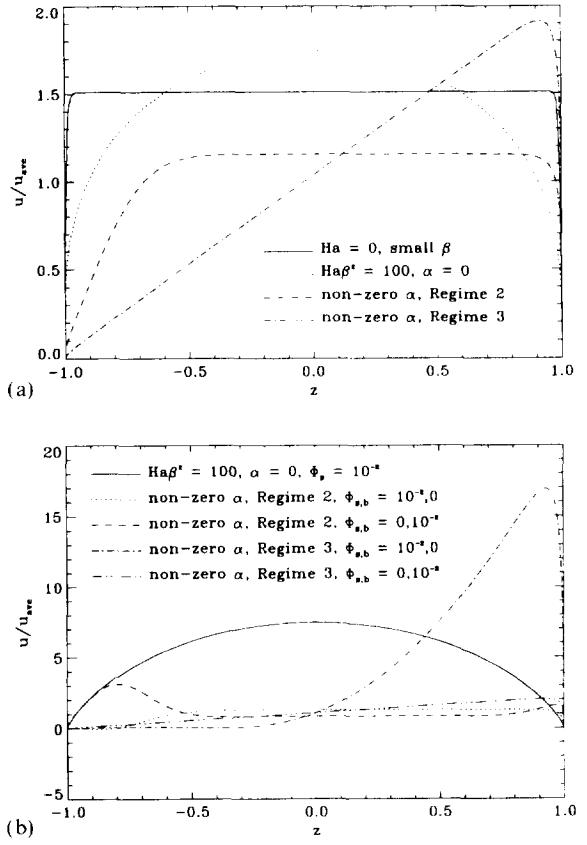

Fig. 4. Velocity profile across the free surface in (a) insulated and (b) conducting channels.

If the boundary layer jet (of approximate thickness $(\mathrm{Ha}\beta^2\cos\alpha)^{-1/2}$ for parallel layers) is very thin, the heated depth may penetrate further into the channel; greater than the jet thickness. The insulated cases with strong MHD interaction have a central core region that is very close to the average velocity used in standard slug flow calculations of heat transfer. This seems a desirable situation. If the flow is not fully core flow, and more parabolic flow (in y) results (regime 1 and transition regimes), this is also favorable since surface velocity is still greater than the average and decreases over the entire depth of the flow, leaving the majority of the flow in the upper half channel.

The equilibrium velocity profile is also important for stability calculations [14]. It is likely that large velocity jets on the surface could be unstable. Should such an instability in velocity and film height develop, provided that it is small in magnitude compared to the total height of the flow, it could positively impact the heat transfer as a mixing layer at the surface could form, providing convection and increasing the heated depth.

The current density, due to Joule dissipation, is also a source of heat for the film flows. Calculations with FDFF have shown that in the limit of high field and/or large β, the film behaves approximately like Hartmann flow in the core region. The current density of total Hartmann flow is (in a dimensional system):

$$|\vec{j}_{\mathrm{core}}| = \Phi_{\mathrm{s}}\sigma_{\mathrm{f}}u_{\mathrm{core}}B\cos\alpha \qquad \text{in regime 3} \tag{22}$$

$$= \Phi_{\mathrm{b}}\sigma_{\mathrm{f}}u_{\mathrm{core}}B\sin\alpha \qquad \text{in regime 2} \tag{23}$$

Since $u_{\mathrm{core}} \leqslant u_{\mathrm{ave}}$ for conducting wall flows, we will use the latter in subsequent equations. The additional volumetric heating in the bulk, due to the flow of current, is approximately computed from the energy equation to be

$$\Delta T_{\mathrm{core}} = L\Phi_{\mathrm{s,b}}^2 u_{\mathrm{ave}}\left(\frac{\sigma_{\mathrm{f}}(B^{\mathrm{a}}\cos\alpha,\sin\alpha)^2}{\rho c_{\mathrm{p}}}\right) \tag{24}$$

$$= 175L\Phi_{\mathrm{s}}^2 u_{\mathrm{ave}} \text{ in regime 3} \tag{25}$$

$$= 12L\Phi_{\mathrm{b}}^2 u_{\mathrm{ave}} \text{ in regime 2} \tag{26}$$

where L is the axial channel length, c_{p} is the heat capacity (about 343 J kg^{-1} °C^{-1} for gallium) and the numerical constant is computed using gallium properties and the maximum field from Table 1. It is possible to envision cases where this heating is appreciable, but for thin conducting or insulated walls (in this case replace Φ with Ha^{-1}), volumetric heating is negligible in the core.

However, if all the core current returns through thin conducting walls, the current density in the wall will be

$$j_{\mathrm{wall}} = \frac{a}{a_{\mathrm{w}}} j_{\mathrm{core}} \tag{27}$$

giving a temperature rise in the wall of

$$\Delta T = \frac{\sigma_{\mathrm{w}}(u_{\mathrm{ave}}B^{\mathrm{a}})^2}{\rho_{\mathrm{w}}c_{\mathrm{w}}} \quad \text{°C s}^{-1} \tag{28}$$

for regime 3 flow. For the worst case parameters given in Table 1, this gives a temperature rise of about 875 °C s^{-1} in a stainless steel wall! This temperature jump, of course, will be moderated by the flow of LM across the channel walls. In addition, it is likely that the flow will not be operating in full regime 3 core flow regime, but in the transition from ordinary hydrodynamic to MHD flow, or in a regime 2 core flow (see Section 3.3). Operating in these regimes will result in a significant reduction in current density and thus a quadratic reduction in local heating near the walls.

The temperature and velocity are necessary to determine the corrosion characteristics of the flowing LM film. Some metals, especially gallium and tin, may be restricted in allowable temperature due to corrosion concerns. The fact that Joule heating may tend to heat the near-wall region, along with the presence of sharp velocity gradients at the walls (seen for most of the flows with strong MHD interaction), may make corrosion an especially critical issue for gallium films when MHD forces are strong.

3.3. Divertor operation at the uniform film height

Although it would be best to create a film with no tendency to vary in height over the entire length of the flow (in other words, at the uniform film height), this is not an absolute requirement if the development length of the flow is long compared to the required channel length. In the presence of a magnetic field though, previous film models (as well as established duct flow models) predict the shortening of the development length as the field increases [4,15]. To help avoid the possibility of dry-out from thinning films, or overfilling from films tending to thicken, it is desirable to design the channel so that h is exactly, or at least near, the desired thickness for divertor operation.

Can a coplanar, LM film divertor be operated at the uniform film height? To help answer this question, Figs. 5 and 6 show the contours of $u_{ave}/\sin\theta$ as a function of channel width and desired film height for several different values of α and wall conductance $\sigma_w a_w$. Notice that these quantities are dimensional, and the non-dimensional tildes will be reinstated in this subsection. The w subscript denotes all channel walls. The wall conductance of the two conducting cases, $\sigma_w a_w = 2000$, is equivalent to a thin metal liner of conductivity 10^6 $(\Omega\,m)^{-1}$ and thickness 2 mm. These specific cases do not cover all possible configurations but serve to show the relevant trends. From these graphs, if the dimensions of the desired film are specified, the value of $u_{ave}/\sin\theta$ that results can be read off. Alternately, if the value of the desired $u_{ave}/\sin\theta$ is determined before hand, the corresponding contour will show the values of h and a that result in such a gallium flow in a 10 T field. As an example of the former case, if the film is desired to be 4 mm in height and 60 cm in width, the value of $u_{ave}/\sin\theta$ for the four cases in Figs. 5 and 6 can be read off and are given in Table 2.

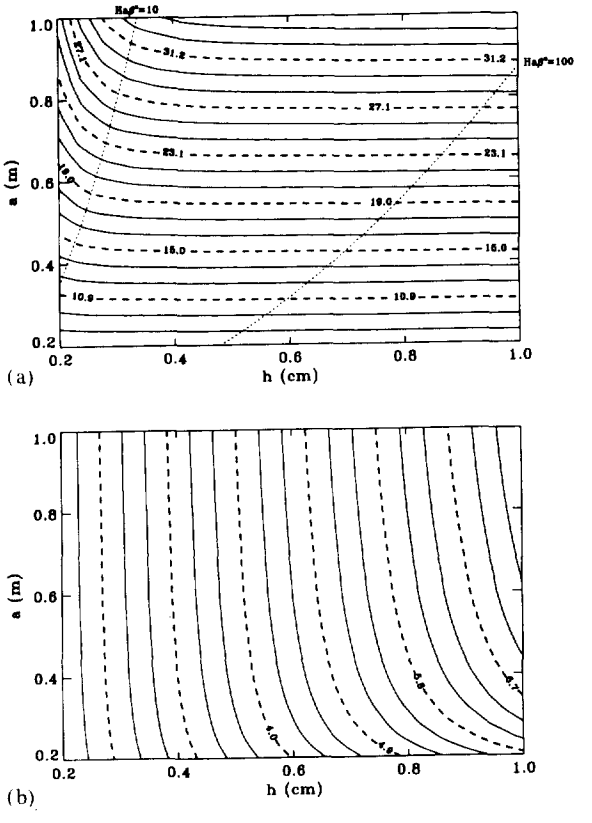

Fig. 5. $u_{ave}/\sin\theta$ in an insulated channel with $B^a = 10$ T: (a) $\alpha = 0°$, (b) $\alpha = 5°$.

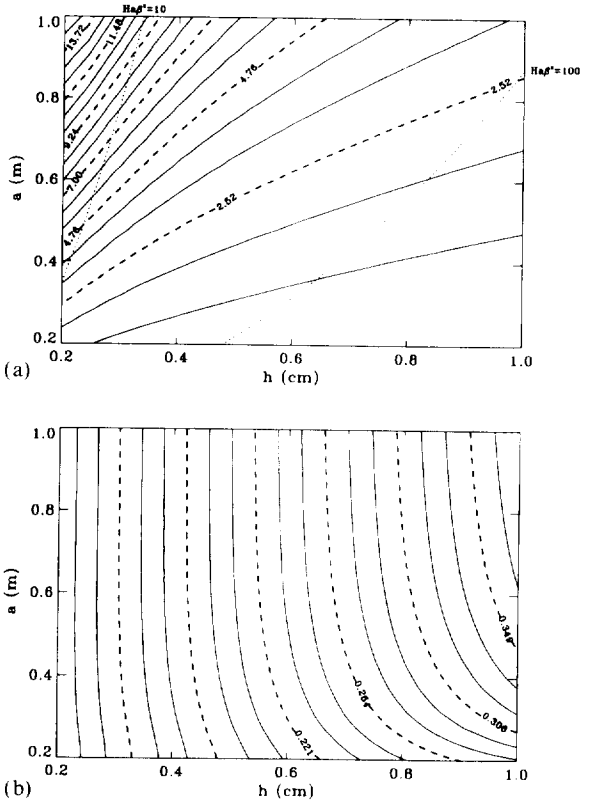

Fig. 6. $u_{ave}/\sin\theta$ in a conducting channel with $B^a = 10$ T, $\sigma_w a_w = 2000$: (a) $\alpha = 0°$, (b) $\alpha = 5°$.

From case 1 it is seen that even if a high speed film of 5 m s^{-1} is necessary for heat removal, that a modest channel angle of only $\theta \approx 14°$ is required. However, neither case 2 nor case 3 will be able to produce a 5 m s^{-1} film velocity, even at steep angles. They can produce a 1 m s^{-1} film, though, at around $\theta = 17°$ and velocities of around 3 m s^{-1} at $\theta = 70°$. (The stability of films flowing at high velocity and steep angles is not a certainty. It is assumed for the sake of this discussion that the field will stabilize such flows to an acceptable degree, but this has not been definitely established.) When both the channel is moderately conducting and the field is oblique, a uniform flow at greater than 0.16 m s^{-1} is not possible at any angle of inclination for the film dimensions given above. At $\alpha = 5°$, a reduction of the wall conductance to 290 is required before even 1 m s^{-1} flow is possible at a 70° inclination.

Table 2
$u_{ave}/\sin\theta$ for $B^a = 10$ T, $h = 4$ mm and $a = 60$ cm

Case	Description	$u_{ave}/\sin\theta$
Case 1	$\alpha = 0°$, $\sigma_w a_w = 0$	20.6
Case 2	$\alpha = 5°$, $\sigma_w a_w = 0$	3.15
Case 3	$\alpha = 0°$, $\sigma_w a_w = 2000$	3.6
Case 4	$\alpha = 5°$, $\sigma_w a_w = 2000$	0.172

Looking at the figures it is possible to understand the qualitative trends with the help of the simple estimations for β as a function of $\tilde{Q}$ (from Refs. [5,8]) summarized here:

$$\beta = \begin{cases} (3\tilde{Q})^{1/3} & \text{A: Ha} = 0,\ \beta \ll 1 \\ \tilde{Q}\text{Ha} & \text{B: Ha}\beta^2 > 10,\ \alpha = 0 \\ (\tilde{Q}\text{Ha}\sin\alpha)^{1/2} & \text{C: Ha},\ \alpha \neq 0,\ \text{regime 2},\ \Phi = 0 \\ \tilde{Q}\text{Ha}\cos\alpha & \text{D: Ha},\ \alpha \neq 0,\ \text{regime 3},\ \Phi = 0 \\ \tilde{Q}\dfrac{\text{Ha}(1+\text{Ha}\Phi_s)}{1+\Phi_s} + \beta_o & \text{E: Ha},\ \Phi \neq 0 \end{cases} \tag{29}$$

where

$$\beta_o = \frac{8}{9}\frac{\Phi_s\sqrt{\text{Ha}}}{1+\Phi_s}\left(1 - \frac{\Phi_b\sqrt{\text{Ha}}}{4(1+\Phi_b\sqrt{\text{Ha}})}\right)$$

for perfectly coplanar films ($\alpha = 0$), but differs for oblique incidence. In Fig. 5(a), the majority of the flow parameter space is in the region greater than $\text{Ha}\beta^2 > 10$ where $\tilde{Q}$ is governed approximately by Eq. (29B). Using this and the definition of $\tilde{Q}$ we can determine that $u_{ave}/\sin\theta$ is independent of h and linearly dependent on a. This is indeed demonstrated in the figure. In the region where $\text{Ha}\beta^2$ is less than 10 we use Eq. (29A) for $\tilde{Q}$ and therefore expect $u_{ave}/\sin\theta$ to be independent of a and vary as h^2. This is also borne out by the figure. Similar reasoning can be used for Fig. 5(b) and Fig. 6 to explain the observed tendencies in the different regions. We notice in particular that in Fig. 5(b) that the above contour tendencies in Fig. 5(a) seem to be reversed. This is because the entire parameter space is solidly in regime 2 flow where the y-field, and not the z-field, dominates the flow. These contour tendencies in Fig. 5(b) start to change in the lower-right corner where

regime 3 flow is approached, and the z-field again makes its presence felt. Explaining the conducting wall graphs gets a little more complicated, as the expressions for β vs. $\tilde{Q}$ contain the Φ parameters which are also dependent on a.

Graphs of this type are useful as design tools to determine possible configurations that allow film flow at the uniform film height. We have seen from the above examples that such flow is possible, especially if an insulated channel is used. In this case, the positive benefits of the field, namely the stabilization of the film flow, are enjoyed while channel flooding due to additional MHD drag is not a problem. The design window becomes tighter as the channel becomes more conducting or the field deviates from z in direction. These conditions result in an increase in the normal film height, and make creating film flows with practical dimensions at a high enough velocity difficult to manage. However, in the coplanar case, flows at $\mathrm{Ha}\beta^2$ around 10 or smaller are not degraded much further than that shown for case 3, no matter how high the wall conductance gets. Conversely, if the substrate is even moderately conducting in regime 2 flows ($\sigma_b a_b > 720$ for $\alpha = 5°$), practical flows at h become impossible, and developing-flow designs must be investigated.

4. Validity of Hartmann-averaging technique

Most previous modeling efforts for fusion-like, quasi-coplanar, thin film flows rely on an averaging method where the velocity of the film as a function of the channel width position (z coordinate) is assumed to be Hartmann. This averaging procedure is described in Ref. [16] and Ref. [8], and is not repeated here. The use of such an averaging technique is attractive since it allows the governing equations to be greatly simplified, to the point where an analytical solution can be found in some cases. Such simple solutions, if accurate, can be used to quickly identify design parameters leading to an acceptable film height and velocity profiles along the divertor, instead of solving complicated systems of equations numerically over all design parameter space.

The two-dimensional FDFF model, since it makes no assumptions about the behavior of the velocity in the z direction, is used to determine if the Hartmann-averaging method can be utilized to accurately determine the velocity profile and uniform film height. To accomplish this, we use several of the models that utilize Hartmann-averaging from the literature for comparison, adapted to this system of non-dimensionalization and reduced to their fully-developed limits. All variables are dimensionless unless specifically noted. The $\langle\ \rangle$ brackets are used to indicate a quantity Hartmann-averaged (H-A) over the width of the channel.

1D parabolic model—based on Aitov et al. [16] which assumes a completely coplanar magnetic field:

$$\beta^3 = Q\left(\mathrm{Ha}\beta^2 + \mathrm{Ha}^2\beta^2\frac{\Phi_s}{1+\Phi_s}\right) + 3Q \tag{30}$$

$$\langle u\rangle = \frac{3Q}{\beta}\left(y - \frac{1}{2}y^2\right) \tag{31}$$

This model uses what we will call method 1 to handle wall conductivity. This method relies on determining the value of the current leaving the fluid and entering the wall by matching Ohm's law and the current conservation equations both in the wall and in the fluid at the interface. Method 1 relies on the assumption that the electric field set up in the core by charge separation is constant in z and drives return current through the sidewalls.

2D-u model—based on Evtushenko et al. [4]:

$$Q = \frac{\beta^3}{m_*^2}\left(1 - \frac{\tanh[m_*]}{m_*}\right) \tag{32}$$

$$\langle u\rangle = \frac{\beta^2}{m_*^2}\left(\tanh[m_*]\sinh[m_* y] - \cosh[m_* y] + 1\right) \tag{33}$$

Again method 1 is used to account for wall conductivity and the parameter $m_*^2 = \mathrm{Ha}\beta^2 + \mathrm{Ha}^2\beta^2[\Phi_s/(1+\Phi_s)]$ can be recognized as the combination of the magnetic terms from the 1D parabolic model.

2D-ub model—based on Baranov et al. [17]:

$$\beta\int_0^1 \langle u\rangle\,\mathrm{d}y = Q \tag{34}$$

$$\frac{\mathrm{d}^2\langle u\rangle}{\mathrm{d}y^2} - \mathrm{Ha}\beta^2\langle u\rangle - 2\mathrm{Ha}^2\beta^2\frac{\Phi_s}{1+\mathrm{Ha}\Phi_s}\langle|b|\rangle = -\beta^2 \tag{35}$$

$$\frac{d^2\langle|b|\rangle}{dy^2} - 2Ha\beta^2 \frac{1+\Phi_s}{1+Ha\Phi_s}\langle|b|\rangle + Ha\beta^2\langle u\rangle = 0 \tag{36}$$

Here the wall conductivity is handled by averaging the magnetic field in addition to the velocity, using the results of the Hartmann problem. This is referred to as method 2. Note that this method is considerably more complicated, resulting in a coupled ODE system instead of analytic solutions.

4.1. Velocity profile comparison

As indicated above, an accurate velocity profile is important for the determination of the heat transfer and temperature profiles in a heated film. Additionally, the average velocity (over the entire channel, not just the Hartmann-averaged width) will determine the uniform film height for a given Q by the relation $\beta = Q/u_{ave}$ (Eq. (14)). The form of the velocity profile, as it turns out, will show the cause of inaccuracy in β predictions due to the inability of the H-A methods to predict parallel layer velocity jets. For this reason, the velocity profiles produced by the H-A models are compared to the FDFF results, which have been averaged over the channel width for this comparison.

Beginning with the case of purely insulated channels, we note that the results from the 2D-ub and the 2D-u models are equivalent, and so only one will be plotted in the following graphical representations. The y direction velocity profiles at several different flowrates, indicative of the weak, medium and strong MHD interaction ranges are shown in Fig. 7. When a value of $Ha\beta^2$ is quoted it refers to the FDFF value of β, since for equal flowrates the values of β can vary drastically between the different models, pointing out poor agreement.

At weak interaction ($Ha\beta^2 \approx 0.5$), good agreement is seen between all the models and the results of the FDFF code. The tendency of the averaged method to slightly overestimate the drag, and hence underestimate the average velocity, is seen. This is due to forcing the boundary layers on the $z = \pm 1$ walls to be very thin

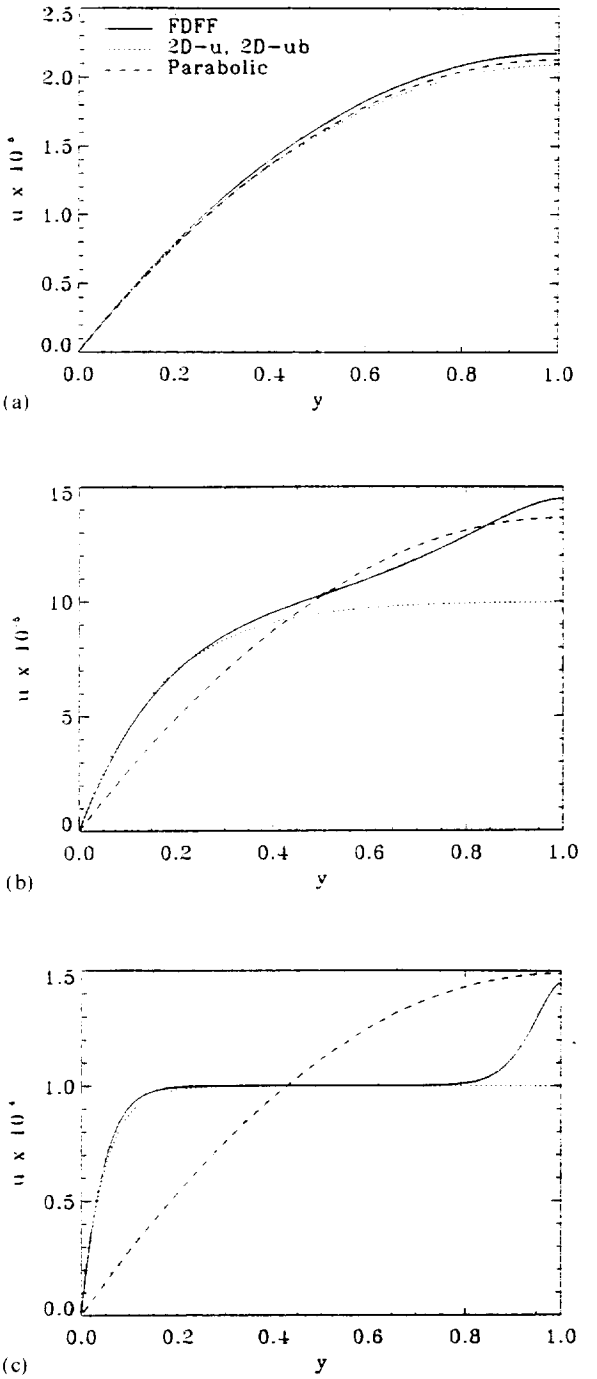

Fig. 7. Comparison of H-A velocity profiles to FDFF results in an insulated channel for $Ha = 10^4$ and Q (or alternatively $Ha\beta^2$) equal to (a) 10^{-7} (0.5), (b) 5×10^{-6} (30) and (c) 2×10^{-5} (400).

(O(Ha^{-1})) instead of the OHD boundary layers (O(β)) predicted by FDFF. The 1D parabolic model gives slightly better agreement than the more complicated 2D models.

In the medium interaction range (Ha$\beta^2 \approx 30$), the velocity is affected by the magnetic field. The underestimation of the average velocity by the 2D model is considerably worse (the 1D parabolic model to a lesser degree), but the average velocity is still of the same order of magnitude as FDFF. However, good agreement is seen between the 2D models and FDFF near the substrate, where a parallel layer is forming in response to the increase MHD interaction.

At strong interaction (Ha$\beta^2 = 400$), the velocity assumes a core flow/parallel layer configuration comparable to duct core flow often seen in the literature. The 1D parabolic model no longer accurately predicts the velocity profile, although the average velocity is still closely predicted. Good agreement in the core region is seen between FDFF and the 2D models. The agreement breaks down near the free surface where the velocity jet is not predicted by 2D-u, which continues flat all the way to the free surface. This is the return current path for the core current, and is not well modeled by the Hartmann-averaging, which is valid only in the core. This large discrepancy is not seen near the substrate since the velocity given by FDFF remains flat as a function of z due to constant friction from the bottom wall. The free surface does not have this constant friction and so the surface jet is parabolic in z (see Fig. 4(a)), vastly different to the flat Hartmann profile. Owing to the absence of the surface jet, the average velocity is still underpredicted by the 2D models, but it is better than the medium interaction case.

As the walls become slightly conducting (Φ_sHa = 1), models 2D-u and 2D-ub are no longer equal. Graphs of the velocity profiles in different interaction regions are provided in Fig. 8. The weak interaction case (not pictured), where little MHD forces are present will be the same as in Fig. 7(a) and is omitted here. At moderate interaction (Ha$\beta^2 = 30$), all the H–A models underestimate the average velocity by a greater amount than the insulated-wall case. Both 2D models track FDFF well near the substrate, but do not handle the beginnings of the velocity jet well near the surface. However, 2D-ub does show a slight increase near the surface where 2D-u is already completely flat.

In the strong interaction regime (Ha$\beta^2 \approx 400$), we see that again the value of velocity in the core region is accurately reflected by the 2D models. In

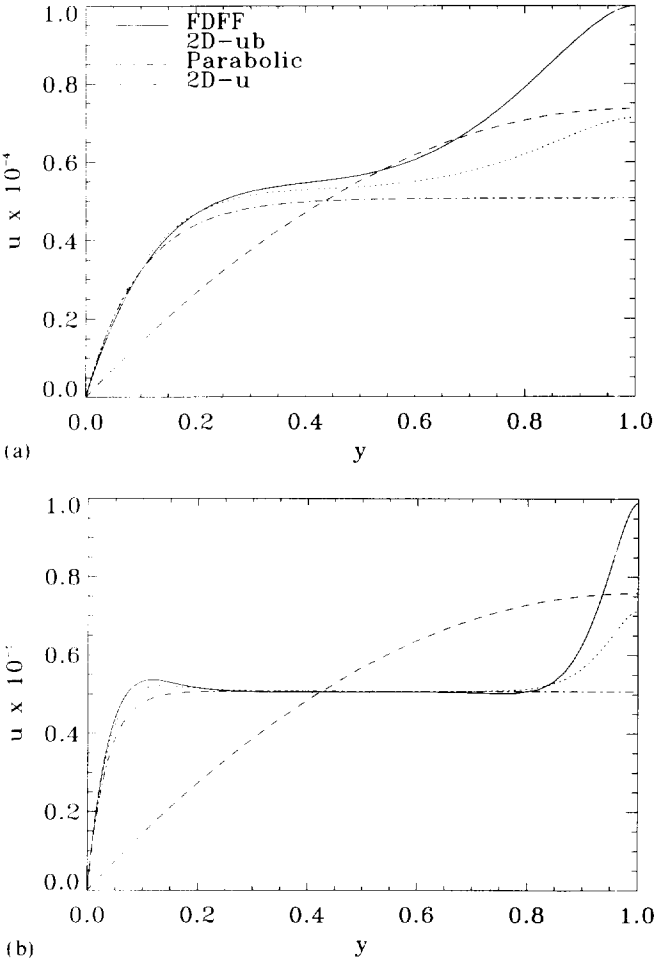

Fig. 8. Comparison of H-A velocity profiles to FDFF results in a poorly conducting (Ha$\Phi_s = 1$) channel for Ha = 10^4, and Q (or alternatively Haβ^2) equal to (a) 3.3×10^{-6} (30) and (b) 10^{-5} (400).

addition, the 2D-ub model predicts a velocity jet both at the free surface and near the substrate. The magnitude of this jet mesured from the core velocity is less than the actual jet by about a factor of 1/2. The average velocity predicted by both 2D models will be less than the actual velocity, but method 2 (accounting for the wall conductivity) seems better able to predict the correct average velocity and gives a closer match to the actual velocity profile. However, for values of $\Phi_c Ha > 1$, the second order central difference program written to solve Eqs. (34)–(36) no longer converges but becomes oscillatory. Some limited analysis of the system of equations indicates that this may be a property of the equations themselves and not the numerical algorithm.

The highly conducting wall cases ($\Phi_c Ha = 100$) are pictured in Fig. 9. For weak interaction in the FDFF results, the 1D and 2D-u models erroneously predict significant interaction. This is a direct result of the Hartmann assumption forcing MHD interaction at very low β due to the contribution of wall conductivity. The inordinately strong MHD effect, and resulting slow average velocity, will give film heights which are far from correct, by over an order of magnitude. The 2D-ub case still converges in the weak interaction case and accurately predicts both the shape of the velocity and the correct average velocity. This means that the onset of the magnetic body force is correctly determined by this model.

In the strong interaction regime ($Ha\beta^2 \approx 400$), it is seen that the core is once again adequately predicted by the H-A technique. However, the large velocity jets which are now carrying an appreciable portion of the flow, are again not predicted. Thus the average velocity is again grossly underestimated and β will be equally as incorrect. The 2D-ub model does not converge in this case.

Of course, the H-A technique assumes the flow to be fully dominated by MHD forces. This is not always a safe bet in wide thin film flow, even at the field strengths representative of magnetic fusion devices. From the point of view of velocity similarity, the H-A technique is unable to predict the formation of velocity jets at the free surface. Depending on the parameters of the flow, this can

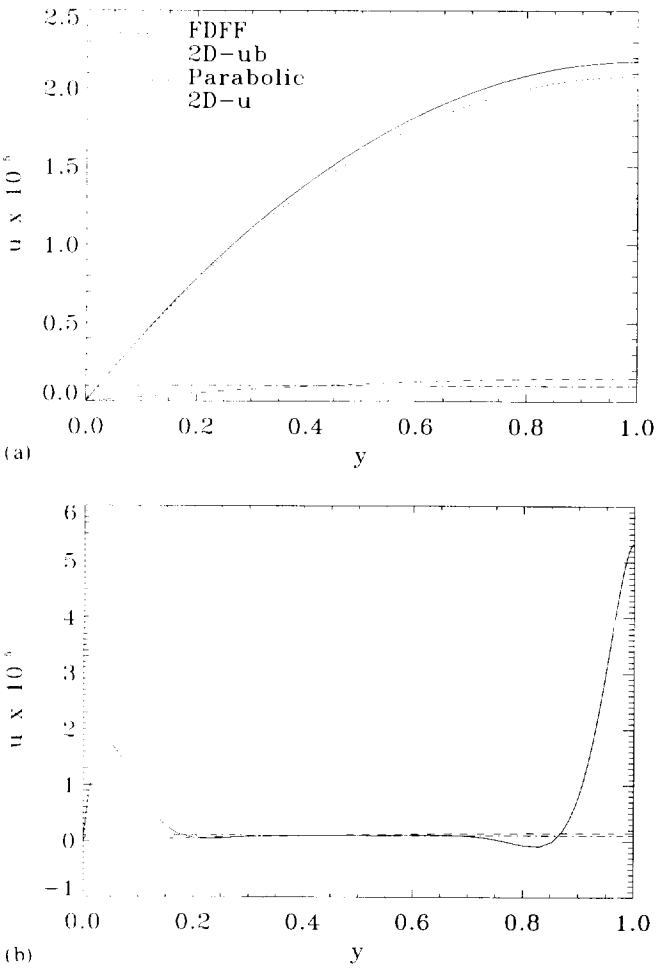

Fig. 9. Comparison of H-A velocity profiles to FDFF results in a highly conducting ($Ha\Phi_c = 100$) channel for $Ha = 10^4$, and Q (or alternatively $Ha\beta^2$) equal to (a) 10^{-7} (0.5) and (b) 10^{-6} (400).

be a significant omission. For insulated channels, discrepancies in velocity profiles do not seem to affect the average velocity prediction to a severe degree, but conducting channels are dramatically affected in all regimes. Method 2 for handling wall conductivity seems to give more realistic results, both in predicting velocity jets and in average velocity determination. Its use, however, above $\Phi_c Ha = 1$ seems to be limited. Method 2 also results in a more complicated system than the simpler u averaging, since a coupled differential equation system must be solved.

Since the velocity jets are parabolically distributed in z, one can envision using a combined Hartmann/parabolic z-profile for averaging the governing equations, thus allowing more accurate simplified solutions for the height and velocity. This in essence is what was done by Shishko [18],

$$u(x, y, z) = \hat{u}(x, y) \cdot (\text{Hartmann} \cdot f(y) + \text{parabolic} \cdot (1 - f(y))) \quad (37)$$

where $f(y)$ varies from zero to one depending on the relative magnitude of the specific profile. Thus, in the surface jet layer f would be close to zero, while in the core region it would be near unity. Shishko's variational method of determining $f(y)$ proved to compare well with FDFF results. The relation for β in the linear region proved accurate as well. However, possibly a simple function for $f(y)$ could be found so that the combo-averaged technique could be used to derive simple relations for developing-film models that reflect to a better degree the velocity profiles that have been determined for fully-developed flow. It should be noted that this comparison was only for purely coplanar fields. The H–A models are not suited to the oblique field case.

4.2. Uniform film height comparison

As seen in the H-A model equations (Eqs. (30)–(36)), the value of β is also determined. Indeed it was necessary to determine the value of β first (or at least concurrently) before solving for the velocity profiles, since the velocity equations require that β be known.

For insulated channels (the β profiles as a function of Q, typical examples shown in Fig. 10), qualitative agreement between all the H-A methods and the FDFF results is seen over the majority of the flowrates considered. This was anticipated in the previous section because the full averaged velocity was seen to be closely predicted by the H-A models. Especially in the weak and strong interaction regimes, good agreement is seen. It is in the medium interaction regime, $\mathrm{Ha}\beta^2 = 10$ to 30, that the largest deviations are seen, because the velocity dependence on z deviates most from the flat Hartmann profile. This deviation is seen in Fig. 11, where the strong and low interactions more closely correspond in shape to the flat Hartmann profile, while the medium regime is more parabolic. Looking back to Fig. 10(b), the maximum deviation in the medium interaction regime is seen to be about 23% and 18% for $\mathrm{Ha} = 10^4$ and 10^5 respectively for the 2D models. The 1D parabolic model gives the best estimation in this region, with the error reduced by a third to a half for the cases examined. Oblique angles result in a much greater deviation, up to a factor of 2 for $\alpha = 5°$.

Conducting walls behave a lot worse in the weak interaction regime. Overestimation of the onset of MHD force has the β overestimated by several orders of magnitude. This situation can be seen in

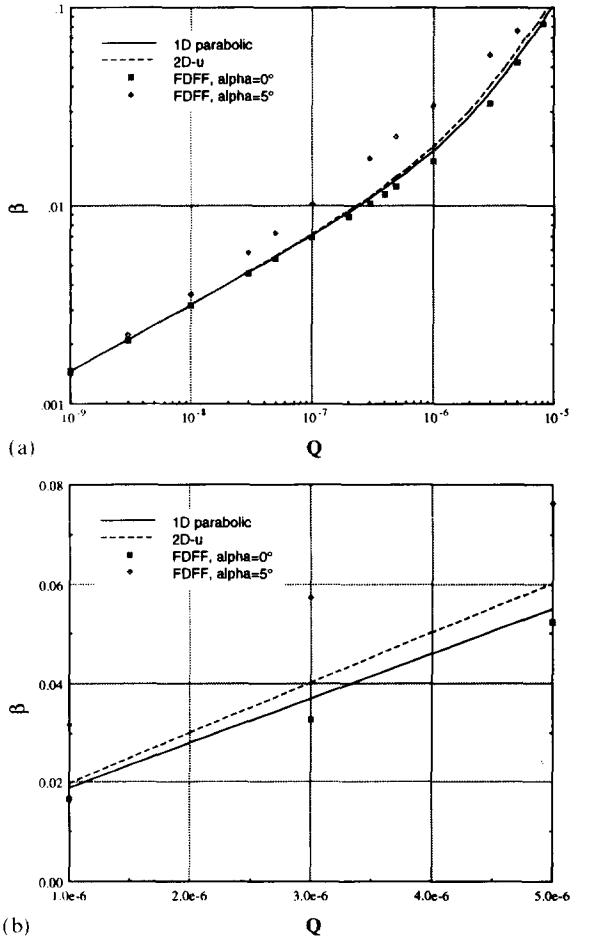

Fig. 10. Comparison of H-A β profiles to FDFF results in insulated channels for $\mathrm{Ha} = 10^4$ for (a) the full range of flowrates and (b) flowrates that give maximum deviation between H–A and FDFF.

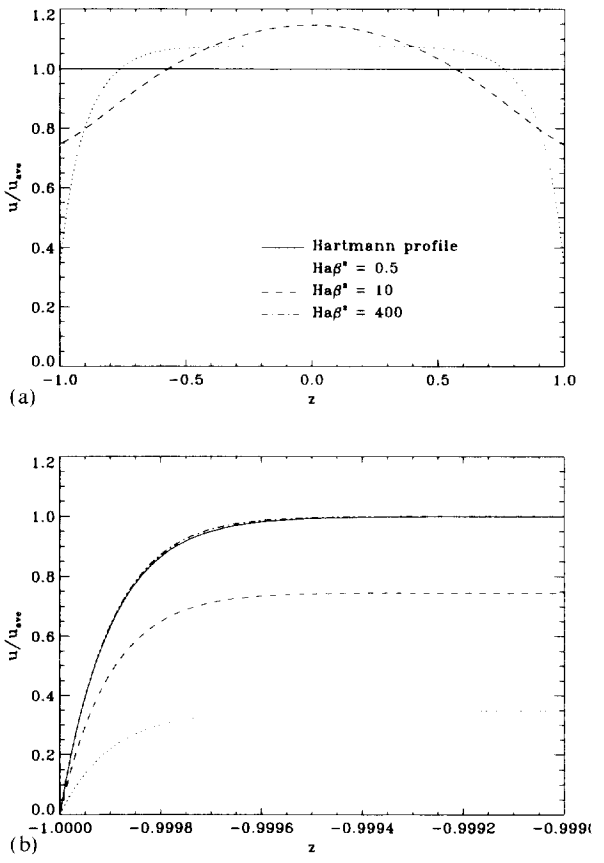

Fig. 11. Comparison of actual z velocity dependence with the Hartmann profile for low, medium and strong interaction regimes: (a) over the whole channel width and (b) near the $z = -1$ sidewall.

Fig. 12 below the jump point in Q. At the jump point, $Q \approx \mathrm{Ha}^{3/2}$, the flow can undergo a rapid reorganization into core flow, accompanied by a jump in film height. Actually, a region of multi-valued β forms in this area, where the film height is likely to jump between competing values (this phenomenon is discussed more thoroughly in Refs. [5,8]). Owing to this jump in β, there is no medium interaction regime to speak off (notice that the medium interacting regime was omitted during the velocity comparisons for high wall conductivity). The jump phenomenon is not predicted by the H-A models. The jump itself can be interpreted by observing the fact that the strong interaction prediction of β is so much larger than that of the weak interaction regime, and so a multiple β region is formed, being large or small depending on the direction of flowrate from which Q_{jump} is approached.

In the strong interaction regime, the value of β predicted by the models differs from the true value by a constant. This constant accounts for the percentage of the flow that is carried out by the parallel layer velocity jets. It is possible to determine a correction for the H-A models by using FDFF to determine the percentage of flow in the parallel layer jets. Thus we see that

$$\beta_{\mathrm{corrected}} = \beta_{\mathrm{uncorrected}} - \frac{8}{9}\frac{\sqrt{\mathrm{Ha}\Phi_s}}{1+\Phi_s} \tag{38}$$

for conducting sidewalls with an insulated substrate. This corrected β is shown in Fig. 12, where

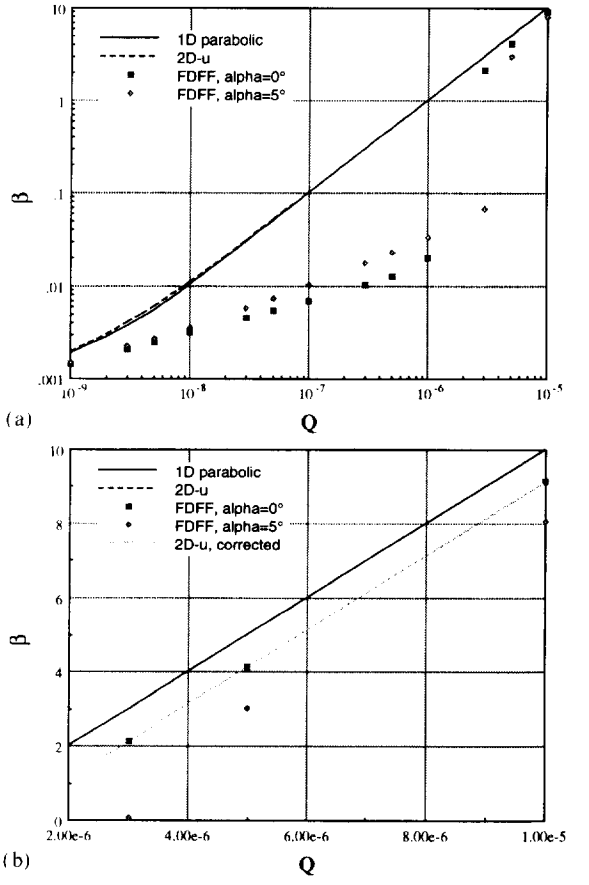

Fig. 12. Comparison of H-A β profiles to FDFF results in conducting ($\mathrm{Ha}\Phi_s = 100$) channels for $\mathrm{Ha} = 10^4$ for (a) the full range of flowrates and (b) flowrates greater than Q_{jump}.

good agreement is seen with FDFF results. Owing to the large values of β in the strong interaction regime, even for Ha at the low end of the range given in Table 1, the practical application of this correction for fusion is in doubt. Flows will have to operate in the weak interaction regime, so that β will not get unacceptably large, if film flow at the uniform film height is required.

When the field angle α is not exactly zero, regime 3 flow can still be generally predicted by the H-A models by substituting Ha cos α for Ha. There is still an error of a constant for conducting channels, this constant being different from that used for the purely coplanar field due to the change in shape of the velocity jets. From Fig. 12 we can estimate the new constant to be 1.88 instead of $\frac{8}{9}$ for the coplanar case. This constant is not as generally accurate for different parameter values as that for coplanar flow because of errors in the estimation of the peak jet velocities.

Regime 2 flow is of a totally different character than regime 3 and the exactly coplanar flows, and should be averaged differently in order to get an accurate representation. In fact, we see in Fig. 5 and Fig. 6 that, for the range of film dimensions considered, the flow is likely to be exclusively in regime 2 when the field angle is around 4–5° or greater. This means that the presence of the toroidal field is superfluous in the computation of the β for a given flowrate (provided that β is small). In this regime then, the whole idea of averaging over the width with a Hartmann profile is simply not the correct approach. Instead, the assumption of an infinitely wide film, with only the y-field component, $B^a \sin \alpha$, retained in the governing equations is more appropriate. Such a model, though even more complex than what is described here, is given in Ref. [15]; unfortunately, this did not appear in the final published version [4]. For films in regime 2, this type of model is more relevant and should be used instead of coplanar film models in design of film divertors.

The conclusion of this section is that in the strong interaction regime, $\mathrm{Ha}\beta^2 > 100$, the Hartmann-averaging technique is successful in predicting the behavior of the core flow when the field is exactly aligned with z. For insulated walls this means that β as a function of Q is predicted with fair accuracy. This accuracy increases with increasing Ha, since the velocity jet at the surface thins, but does not increase in magnitude. For α slightly larger than zero, β is still adequately predicted by using only the z component of the field in Ha. This is true only for regime 3, where the flow is dominated by z; in regime 2 the character of the flow is different and should be treated as wide open flow with no sidewalls. For conducting walls, the flow quantity in the parallel layer jets can carry a significant portion of the total flow, this jet is not predicted by the H-A models, except model 2D-ub which is limited in practical range of wall conductance. The lack of the surface jet results in an overprediction of β. A correction term that takes into account the size of the velocity jets is given in Eq. (38) and works well for flows past the jump value of Q.

5. Concluding remarks

The application of a fully-developed, MHD, open-channel flow model to evaluate the prospect of protecting the surface of a tokamak divertor has been discussed. It is difficult to summarize all the points of interest in this paper due to the variety of different phenomena discussed. In general, an attempt to list the significant conclusions was included at the end of each section. Most important is the observation that flows in the complicated field geometries near the divertor will likely be of the regime 2 type, where the main flow variables will be determined by the effect of the smaller y component of the external magnetic field, rather than the larger z component. The applicability of the Hartmann-averaging technique to this regime is inappropriate. Even for regime 3 flow, the Hartmann-averaging technique tends to overestimate the film height due to its failure to predict the flow in parallel layer velocity jets. This is especially true for electrically conducting channels, where these jets can be large. The accuracy of the averaging technique is increased

in regime 3 if a combination of parabolic and Hartmann profiles are used to average the governing equations.

Acknowledgements

The authors wish to thank Mark S. Tillack and Evgeni Murav'ev for many helpful discussions and editorial suggestions. This work was partially supported by a Magnetic Fusion Energy Technology Fellowship administered for the US Department of Energy at the Oak Ridge Institute for Science and Education.

Appendix A: Nomenclature

a	channel width with walls at $\pm a/2$ (m)
$\tilde{b}$	dimensionless x component of induced magnetic field, $B'_x/u_* \mu_m (\sigma_f \nu \rho)^{1/2}$
$\vec{B}^{i,a}$	induced or applied magnetic induction (T)
FDFF	fully-developed film flow
g	acceleration of gravity (m s^{-2})
h	uniform (fully-developed) flow height (m)
Ha	Hartmann number, $B(a/2)(\sigma_f/\rho\nu)^{1/2}$
$\tilde{Q}$	dimensionless flowrate, $Q/(2(a/2)^4 g \sin\theta/\nu)$
Re	Reynolds number $(u_{ave} h/\nu)$
$\tilde{u}$	dimensionless velocity, $u/(a/2)^2 g \sin\theta/\nu$ (m s^{-1})
$\vec{v}$	fluid velocity, $\vec{v} = [u, v, w]$ (m s^{-1})
x	coordinate along the main direction of the flow (longitudinal)
y	coordinate normal to film substrate (transverse)
z	coordinate perpendicular to flow but in the plane of the substrate (coplanar)
$\langle\ \rangle$	channel width average brackets

Greek letters

α	angle of applied magnetic field to z
β	normalized film height, $h/(a/2)$
Φ	wall conductance ratio, $\sigma_w a_w/\sigma_f(a/2)$
μ_m	magnetic permeability (H m^{-1})
ν	kinematic viscosity (m^2 s^{-1})
ρ	mass density (kg m^{-3})
$\sigma_{f,w}$	fluid, wall electrical conductivity $(\Omega\ \mathrm{m})^{-1}$
θ	angle of channel to horizon
$\omega_\pm$	combined flow functions, $\tilde{u} \pm \tilde{b}$

References

[1] B. Badget et al., Wisconsin torodial fusion reactor design study, Technical Rep. UWFDM-68, Vol. 2, 1974, pp. III-D-1–5 (University of Wisconsin, Madison).

[2] C.P. Liao, M.S. Kazami and J.E. Meyer, Hydrogen transport and edge plasma modeling of liquid metal divertors, Fusion Technol. 23(2) (1993) 208–217.

[3] N.B. Morley, A.A. Gaizer and M.A. Abdou, Estimates of the effect of a plasma momentum flux on the free surface of a thin film of liquid metal, Fusion Eng. Des. 28 (1995) 176.

[4] I.A. Evtushenko, S.Y. Smolentsev and A.V. Tananaev, Hydrodynamics and exchange of heat in thin liquid-metal layers within a magnetic field, Magnetohydrodynamics 27(3) (1991) 287–291.

[5] N.B. Morley and M.A. Abdou, Study of fully-developed, liquid metal, film flow in a nearly coplanar magnetic field, submitted to Int. J. Multiphase Flow.

[6] H. Branover, Magnetohydrodynamic Flows in Ducts, Israel University Press, Jerusalem, 1978.

[7] E.V. Murav'ev, Film MHD flow under conditions of a thermonuclear reactor, Magnetohydrodynamics 24(1) (1988) 125–138.

[8] N.B. Morley, Numerical and experimental modeling of liquid metal, thin film flow in a quasi-coplanar magnetic field, Ph.D. Thesis, University of California, Los Angeles, 1994.

[9] S. Patankar, Numerical Heat Transfer and Fluid Flow, McGraw-Hill, New York, 1981.

[10] P. Roberts and N.B. Morley, Solutions of uniform, open-channel, LM MHD flow in a strong, oblique magnetic field, submitted to Phys. Fluids.

[11] E.V. Murav'ev, Liquid metal devices for systems of impurity control and first wall shielding in tokamak thermonuclear reactors, All-Union Conf. on Engineering Problems of Thermonuclear Reactors, ANL-TRANS-89-4, USSR, January, 1984.

[12] N.B. Morley, M.S. Tillack and M.A. Abdou, Analysis of LM thin film protection of fusion reactor limiter–divetor surfaces, Fusion Technol. 19(3) (1991) 1765–1771.

[13] C.P. Liao and M.S. Kazami, A feasibility assessment of liquid metal divertors, Fusion Technol. 21(3) (1992) 1845–1851.

[14] N.B. Morley and M.S. Tillack, Examination of stability calculations of LM thin film flows in a coplanar magnetic field, Magnetohydrodynamics 29(2) (1993) 69–75.

[15] I.A. Evtushenko, S.Y. Smolentsev and A.V. Tananaev, Hydrodynamics and heat transfer in thin liquid-metal layers within a magnetic field, unpublished draft in English, 1990.

[16] T.N. Aitov, A.B. Ivanov and A.V. Tananaev, Flow of liquid metal in a chute in a coplanar magnetic field, Magnetohydrodynamics 23(1) (1987) 91–95.

[17] V.V. Baranov, I.A. Evtushenko, I.R. Kirillov, E.V. Firsova and V.V. Yakovlev, Liquid metal film flow for fusion application, Seventh Beer-Sheva Int. Seminar on MHD Flows and Turbulence, February, 1993.

[18] A. Shishko, A theoretical investigation of steady-state film flows in a coplanar magnetic field, Magnetohydrodynamics 28(2) (1992) 170–182.